

Zeolitic imidazolate framework-coupled resonators for enhanced gas detection

This content has been downloaded from IOPscience. Please scroll down to see the full text.

2013 J. Micromech. Microeng. 23 125027

(<http://iopscience.iop.org/0960-1317/23/12/125027>)

View [the table of contents for this issue](#), or go to the [journal homepage](#) for more

Download details:

IP Address: 131.243.19.88

This content was downloaded on 04/01/2014 at 02:24

Please note that [terms and conditions apply](#).

Zeolitic imidazolate framework-coupled resonators for enhanced gas detection

Yongha Hwang^{1,6}, Anh Phan², Kosmas Galatsis³, Omar M Yaghi⁴
and Rob N Candler^{1,5}

¹ Electrical Engineering Department, University of California, Los Angeles, California 90095, USA

² Molecular and NanoArchitecture Center, Ho Chi Minh, Vietnam

³ Department of Materials Science and Engineering, University of California, Los Angeles, California 90095, USA

⁴ Department of Chemistry, University of California, Berkeley, California 94720, USA

⁵ California NanoSystems Institute, University of California, Los Angeles, California 90095, USA

E-mail: hwangyongha@ucla.edu

Received 11 June 2013, in final form 12 September 2013

Published 14 November 2013

Online at stacks.iop.org/JMM/23/125027

Abstract

This work presents for the first time a zeolitic imidazolate framework (ZIF)-coupled resonant gas sensor whose sensitivity shows an improvement up to 78 times over bare silicon resonant sensors with identical dimensions. ZIFs are among the highest surface area material used for resonant-based sensing. We utilize high surface area-to-volume ratios of ZIFs to demonstrate how a microresonator coupled with ZIF crystals can provide high sensitivity to chemical vapors.

(Some figures may appear in colour only in the online journal)

1. Introduction

Resonant sensors can detect chemical and biological analytes by measuring shifts in the resonant frequency (f_0) due to adsorption-induced mass changes. The change in the resonant frequency (Δf) is given by

$$\Delta f = -\frac{1}{2} \frac{\Delta m}{m} f_0. \quad (1)$$

Hence, either increasing the adsorbed mass (Δm) or decreasing the resonator mass (m) results in improved sensitivity (i.e., larger fractional frequency shifts ($\Delta f/f_0$)). Substantial research has been undertaken in exploring the fundamental limits of resonant sensors to detect mass with zeptogram resolution [1] and quantum ground state [2]. These fundamental studies require ultra-high vacuum (10^{-8} Pa) and/or extremely low temperatures (25 mK) to achieve low noise for improved resolution. As (1) shows, miniaturizing sensors toward nanometer dimensions (i.e., reducing the resonator mass) improves their sensitivity. However, device scaling does create some challenges. For example, ultra-small sensors have smaller capture areas, so analyte molecules take

a longer time to accumulate on the sensor. This problem is most pronounced when detecting low concentrations of analytes [3] and requires the application of specific methods such as the precise control of the flux of analytes [1]. Smaller resonant devices also tend to have lower quality factors [4], and resolution degrades with the decreasing quality factor. In this work, we describe a sensing approach that provides the sensitivity of nanoscale devices without sacrificing the capture area through the use of highly porous zeolitic imidazolate frameworks (ZIFs) (i.e., increasing the adsorbed mass). The ZIFs also provide potential for high selectivity to desired analytes.

ZIFs are a new class of three-dimensional crystalline structures synthesized from the transition metals bridged by imidazolate. The high surface area and tailorable nanoporosity of ZIFs are attractive for various sensing methodologies, such as the detecting changes of impedance, refractive index, and strain [5–7]. This work demonstrates resonant sensors coupled with ZIFs, which is significant as ZIFs are among the largest surface area materials used for resonant sensing. As an example, ZIF-69, has a high Langmuir surface area of $1070 \text{ m}^2 \text{ g}^{-1}$ and a high affinity for CO_2 , enabling superior adsorption and selectivity properties [8].

⁶ Author to whom any correspondence should be addressed.

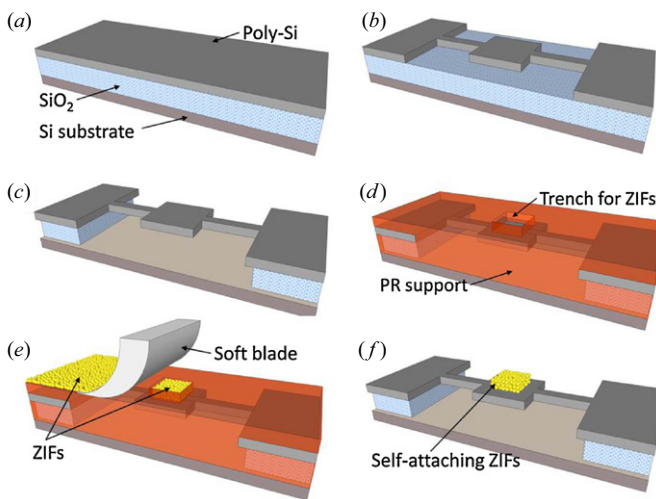


Figure 1. A fabrication process for the ZIF-coupled resonator. (a) Depositing SiO_2 and polysilicon. (b) Patterning body of the resonator. (c) Etching the SiO_2 sacrificial layer. (d) Patterning the photoresist support structure as a second sacrificial layer and trench for a target region of ZIF particles. (e) Drop-casting ZIF particles. (f) Releasing the resonator.

2. Experiments

As shown in figures 1 and 2, the ZIF-coupled microresonators consist of $0.47\text{-}\mu\text{m}$ thick, $45\text{-}\mu\text{m}$ long, $10\text{-}\mu\text{m}$ wide torsional beams, a $45\text{-}\mu\text{m}$ long, $45\text{-}\mu\text{m}$ wide center paddle and a target region in the center paddle to which the ZIFs are attached. When coupling resonators with ZIFs, careful fabrication considerations must be made as ZIFs are damaged at temperatures greater than $390\text{ }^\circ\text{C}$ or in the acidic solutions (e.g., hydrofluoric acid). Therefore, the use of acid to etch a sacrificial layer, which is required to produce a free standing resonator, must occur before the assembly of the ZIFs. The resonators here are fabricated using sublimation drying with p-DCB (p-dichlorobenzene) and a two-step sacrificial layer process in combination with standard surface micromachining processes [9]. ZIF-69 nanoparticles are assembled into the pre-patterned target regions by a drop-casting method, which is preferred here for its flexibility to assemble a variety of materials.

The process starts with the deposition of $5.5\text{-}\mu\text{m}$ thick silicon dioxide (SiO_2) as the first sacrificial layer, followed by

the deposition of a 470-nm thick polysilicon structural layer (figure 1(a)). After defining the resonator (figure 1(b)), the SiO_2 sacrificial layer is removed by immersing wafers in the hydrofluoric acid solution, followed by rinsing with deionized (DI) water (figure 1(c)). From this moment, careful handling is necessary as resonators are released from the substrate. To form the second sacrificial layer right after removing the first one, the following unique series of immersion steps are performed (figure 1(d)). First, DI water is replaced with methanol, a low surface tension solvent. Methanol is then replaced with the melted sublimation liquid, p-DCB. Once the p-DCB starts to solidify at room temperature, photoresist (PR) (AZ 4620) is immediately poured over the p-DCB, which is required because the solidified p-DCB rapidly begins to sublime. Finally, the solid p-DCB under the released structures sublimates in a vacuum chamber. While simultaneously the p-DCB is fully sublimated, the device will be completely underfilled and covered by the PR. The thick PR is patterned using conventional photolithography techniques into a mold for ZIFs. The PR layer plays dual roles in this process, acting as both the second sacrificial layer by providing support underneath the resonator and a mold for ZIFs on top of the resonator.

In an ultrasonic bath, the ZIFs are suspended in DI water and then loaded onto the top surface of the PR mold. A flat blade is used to sweep across the surface of the mold and pack the ZIFs into the pre-patterned trenches $3\text{ }\mu\text{m}$ deep, ensuring the agglomeration and attachment of the ZIFs onto the center paddle of the resonator (figure 1(e)). Finally, the PR is removed with acetone to release the ZIF-coupled resonator, and the sublimation drying of p-DCB is performed again to avoid stiction. The second sublimation drying procedure does not prevent the nanoparticles from providing the enhanced surface area for adsorption, as it is performed at relatively low temperature ($\sim 65\text{ }^\circ\text{C}$) and adsorbed p-DCB is completely removed by sublimation in a vacuum desiccator for 3 h. The ZIFs adhere onto the silicon surface without an adhesive layer, possibly a result of van der Waals forces [10]. Since no adhesive binders are required unlike a typical drop-casting technique [11], the ZIF nanoparticles have maximum exposure to the surrounding environment to ensure the maximum physical adsorption of analytes.

The frequency spectra of the resonant gas sensors were measured with a test setup that consists of a laser doppler

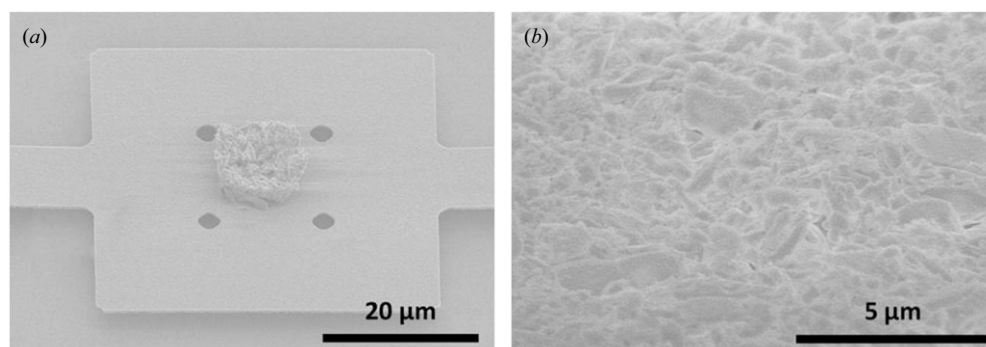


Figure 2. SEM images. (a) Resonator with a $10 \times 10 \times 3\text{ }\mu\text{m}^3$ casting of ZIFs. (b) An enlarged image of ZIFs attached on the surface of the resonator.

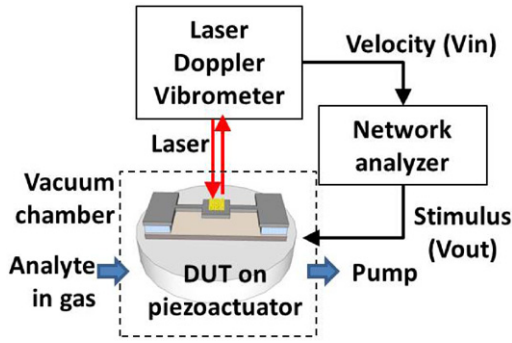


Figure 3. A schematic diagram of a test setup. Device under test (DUT) is actuated by a piezoelectric actuator, and resonance is detected using a laser doppler vibrometer and network analyzer.

vibrometer (LDV, Polytec OFV-5000), a custom-built vacuum chamber, and a network analyzer (HP 8753D) as shown in figure 3. Mechanical vibration is induced by an external piezoelectric actuator, which is controlled by the stimulus signal of the network analyzer. The frequency response is measured by the LDV.

To estimate the ZIF sensing properties, control experiments are performed using silicon resonators without ZIFs, which will be subsequently referred to as the bare silicon resonators. The measured short-term frequency noise floor and the quality factor of the resonators are shown in figure 4. The frequency stability of the entire setup is characterized by the Allan deviation, defined as

$$\langle \delta f_0 / f_0 \rangle_\tau = \sqrt{\frac{1}{(N-1)} \sum_{i=1}^N \left(\frac{\bar{f}_{i+1} - \bar{f}_i}{f_0} \right)^2}, \quad (2)$$

where \bar{f}_i is the average frequency in the i th time interval τ , and N is the number of independent frequency measurements [12]. The Allan deviations of the resonant frequencies of the ZIF-coupled and the bare silicon resonator are 2.9×10^{-5} and 8.7×10^{-6} over a 10 s integration time, respectively. The presence of ZIFs on the resonators reduces the quality factor by a factor of 3. Temperature-induced frequency drift for silicon resonators is one possible noise source, as the temperature dependence of Young's modulus causes a frequency shift [13]. Also, a mismatch of the thermal expansion coefficient of an additional material (i.e., ZIFs in this work) on the silicon resonator might induce stress, resulting in a frequency shift and a degradation in the quality factor [14]. The minimum detectable mass is calculated as $\delta M = 2m_{\text{eff}} \langle \delta f / f_0 \rangle_\tau$, where m_{eff} ($\sim 2.39 \times 10^{-9}$ g) is the effective mass by means of Rayleigh's principle [15]. Hence, the limit of detection of the ZIF-coupled resonator for gas sensing is expected to be ~ 0.13 pg, and the corresponding gas concentration is approximately 15 ppm of CO₂.

Figure 5 contains characteristic frequency shifts showing real time frequency measurements under different gas conditions. Vapor concentrations are measured in partial pressure of the chamber, for which the base pressure is 5 Pa. The responses are repeatedly recovered to their baseline values upon the removal of gas, indicating reversible adsorption. The

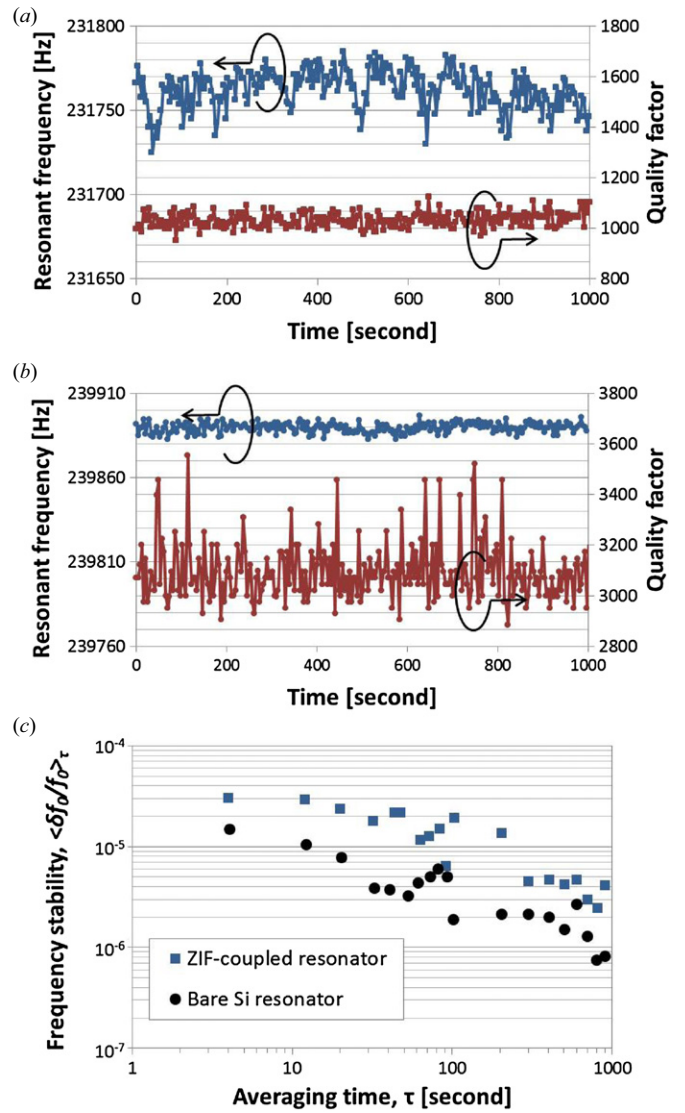


Figure 4. Measured noise floor and Q factors of the systems with (a) the ZIF-coupled resonator and (b) the bare silicon resonator during 1000 s measurement period. (c) Allan deviation measured in the open loop condition.

different gas types may have different adsorption time delay because ZIFs can be designed to store particular gases [8, 16]. Customized design of ZIFs could enable enhanced sensitivity for target gases.

Figure 6 shows $\Delta f / f_0$ resulting from the adsorption and desorption of different gases for the bare silicon resonators and ZIF-coupled resonators. Whereas the frequency shifts of the bare silicon resonator without ZIFs during the gas adsorption are almost negligible due to the insufficient adsorption, the resonant frequency of the ZIF-coupled resonators changes substantially due to the increase in the surface area afforded by assembled ZIFs. The process flow was designed to avoid adhesive binders that could clog the ZIFs, enabling this enhanced sensitivity to be realized. Nevertheless, the accumulation of gas on the ZIFs is likely to inhibit further adsorption at some point, leading to saturation and reduced sensitivity at higher concentrations.

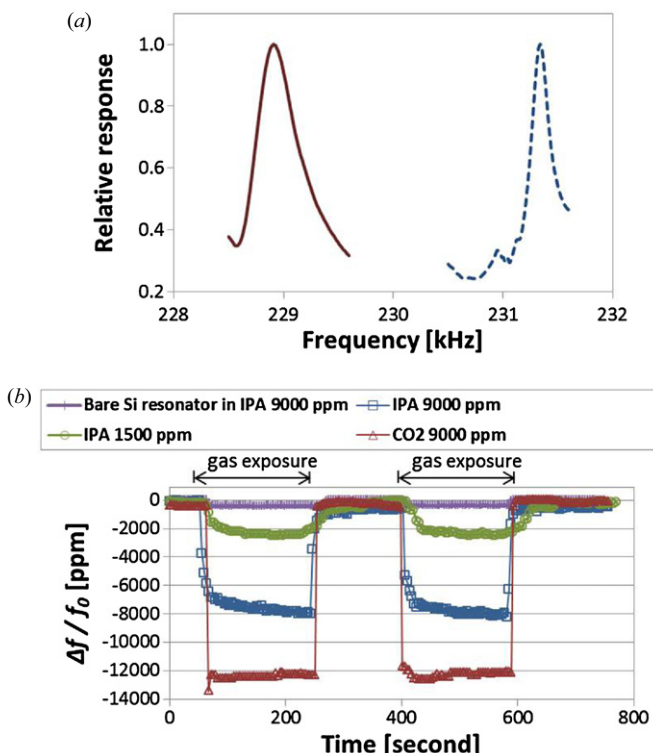


Figure 5. Measured performance of the ZIF-coupled resonant gas sensors. (a) Frequency spectra of the ZIF-coupled resonator with no CO₂ (dashed line) and 9000 ppm of CO₂ (solid line). (b) A typical set of real time frequency shifts exposed to IPA and CO₂ gas.

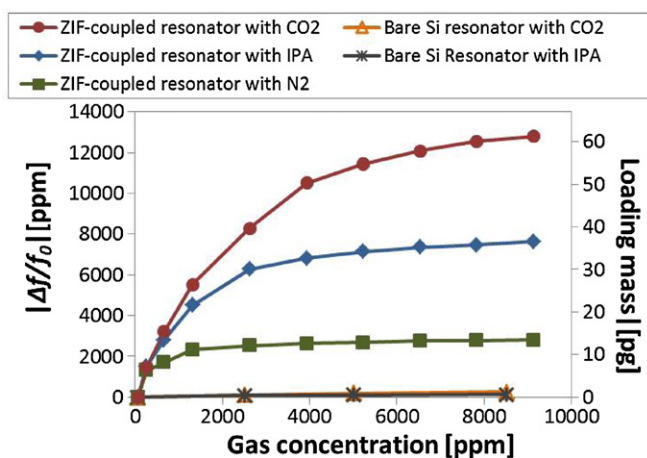


Figure 6. Response of the ZIF-coupled resonant gas sensors to N₂, IPA and CO₂ gas given in terms of both frequency shift and equivalent loading mass.

As a result, the ZIF-coupled resonators show higher frequency shifts ranging between 32 and 78 times for different gas concentrations compared to resonators without ZIFs. Furthermore, because of the inherent selectivity of ZIFs [8], the ZIF-coupled resonator has 1.7 times higher sensitivity to CO₂ than IPA in spite of the lighter molar mass of CO₂. Assuming that the frequency shift is affected only by the mass change, the mass adsorbed on ZIF-coupled resonator for a CO₂ concentration of 2500 ppm is calculated to be 40 pg from equation (1), as shown in figure 6. As an aerial mass of

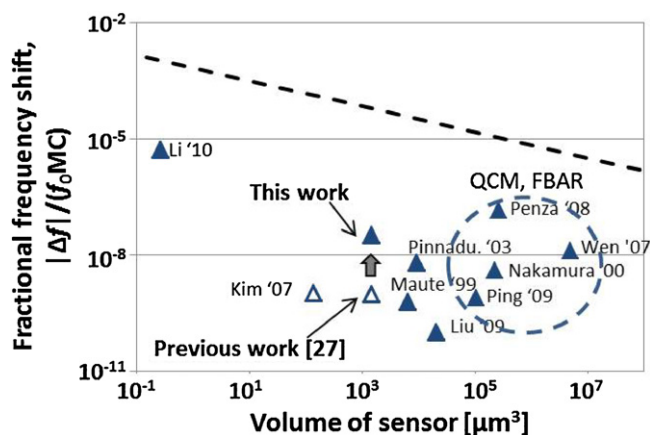


Figure 7. Frequency shift (Δf) from adsorbed gas, normalized by resonant frequency (f_0), molar mass (M) and concentration (C) of gas, plotted against resonator volume. Most of the compared works (the filled triangles) also employed additional functionalized layers for enhancing sensitivity and selectivity. Points inside the dotted circle utilized QCM (quartz crystal microbalance), SAW (surface acoustic wave) or FBAR (film bulk acoustic resonator) platforms [18–26]. Others are beam-type resonators. This work achieves sensitivity improvement 32 times over the previous work using porous silicon [27].

CO₂ is calculated as 28 ng cm⁻² [17], the amount adsorbed onto the ZIF-coupled resonator corresponds to 29 monolayers on the silicon resonator surface of 4900 μm², which implies the adsorption of the ZIF-coupled resonator occurs not only on the surface but also inside the ZIFs as desired. Therefore, the ZIFs enhance the surface area for the gas detection, enabling the sensitivity of the gas sensor to be improved.

Figure 7 shows the overall trend of size dependence of sensitivity in resonant gas sensors [18–26]. The ZIF-coupled resonator provides improved sensitivity for structures with dimensions around 10 s of μm. This size scale is of interest because it is small enough to enable the arrays of devices for applications such as electronic noses and is large enough to provide the sufficient capture area for the low concentration detection. This work achieves sensitivity improvement 32 times over the previous work using porous silicon and 78 times over the bare silicon resonators [27].

3. Conclusion

This study demonstrated sensitivity improvement of the chemical vapor detection using the ZIF-coupled resonators, which have ultra-high surface area as compared to solid resonators. By using a microscale device with nanoscale features, we have leveraged the best of both size scales (i.e., the microscale capture area with nanoscale sensitivity). ZIF materials hold the promise of tunable sensitivity by the variety of organic linkers they can have. Therefore, a diverse class of ZIF materials can be assembled using the drop-casting method, making resonators useful for a wide variety of adsorption-based sensing applications.

Acknowledgments

This work was supported in part by the Broadening Participation Research Initiation Grants program of the National Science Foundation under Award #0926228 and by the Focus Center for Functional Engineered Nano Architectonics.

References

- [1] Yang Y T, Callegari C, Feng X L, Ekinci K L and Roukes M L 2006 Zeptogram-scale nanomechanical mass sensing *Nano Lett.* **6** 583–6
- [2] O'Connell A D *et al* 2010 Quantum ground state and single-phonon control of a mechanical resonator *Nature* **464** 697–703
- [3] Sheehan P E and Whitman L J 2005 Detection limits for nanoscale biosensors *Nano Lett.* **5** 803–7
- [4] Yasumura K Y, Stowe T D, Chow E M, Pfafman T, Kenny T W, Stipe B C and Rugar D 2000 Quality factors in micron- and submicron-thick cantilevers *J. Microelectromech. Syst.* **9** 117–25
- [5] Allendorf M D, Houk R J T, Andruszkiewicz L, Talin A A, Pikarsky J, Choudhury A, Gall K A and Hesketh P J 2008 Stress-induced chemical detection using flexible metal-organic frameworks *J. Am. Chem. Soc.* **130** 14404
- [6] Achmann S, Hagen G, Kita J, Malkowsky I M, Kiener C and Moos R 2009 Metal-organic frameworks for sensing applications in the gas phase *Sensors* **9** 1574–89
- [7] Lu G and Hupp J T 2010 Metal-organic frameworks as sensors: a ZIF-8 based fabry—pérot device as a selective sensor for chemical vapors and gases *J. Am. Chem. Soc.* **132** 7832–3
- [8] Banerjee R, Phan A, Wang B, Knobler C, Furukawa H, O'Keeffe M and Yaghi O M 2008 High-throughput synthesis of zeolitic imidazolate frameworks and application to CO₂ capture *Science* **319** 939–43
- [9] Hwang Y-H and Candler R N 2012 Fabrication process for integrating nanoparticles with released structures using photoresist replacement of sublimated p-dichlorobenzene for temporary support *J. Microelectromech. Syst.* **21** 1282–4
- [10] Hartley P A, Parfitt G D and Pollack L B 1985 The role of the van der Waals force in the agglomeration of powders containing submicron particles *Powder Tech.* **42** 35–46
- [11] Wang N, Bowers B J and Arnold D P 2008 Wax-bonded NdFeB micromagnets for microelectromechanical systems applications *J. Appl. Phys.* **103** 07E109
- [12] Feng X L, White C J, Hajimiri A and Roukes M L 2008 A self-sustaining ultrahigh-frequency nanoelectromechanical oscillator *Nature Nanotechnol.* **3** 342–6
- [13] Tudor M J, Andres M V, Foulds K W H and Naden J M 1988 Silicon resonator sensors: interrogation techniques and characteristics *IEEE Proc. D* **135** 364–8
- [14] Shen F, Lu P, O'Shea S J, Lee K H and Ng T Y 2001 Thermal effects on coated resonant microcantilevers *Sensors Actuators A* **95** 17–23
- [15] Lobontiu N, Ilic B, Garcia E, Reissman T and Craighead H G 2006 Modeling of nanofabricated paddle bridges for resonant mass sensing *Rev. Sci. Instrum.* **77** 073301
- [16] Phan A, Doonan C J, Uribe-Romo F J, Knobler C B, O'Keeffe M and Yaghi O M 2010 Synthesis, structure, and carbon dioxide capture properties of zeolitic imidazolate frameworks *Acc. Chem. Res.* **43** 58–67
- [17] Furukawa H *et al* 2010 Ultrahigh porosity in metal-organic frameworks *Science* **329** 424–8
- [18] Li M, Myers E B, Tang H X, Aldridge S J, McCaig H C, Whiting J J, Simonson R J, Lewis N S and Roukes M L 2010 Nanoelectromechanical resonator arrays for ultrafast, gas-phase chromatographic chemical analysis *Nano Lett.* **10** 3899–903
- [19] Kim S J, Ono T and Esashi M 2007 Mass detection using capacitive resonant silicon resonator employing LC resonant circuit technique *Rev. Sci. Instrum.* **78** 085103
- [20] Pinnaduwa L A, Boiadjev V, Hawk J E and Thundat T 2003 Sensitive detection of plastic explosives with self-assembled monolayer-coated microcantilevers *Appl. Phys. Lett.* **83** 1471–3
- [21] Maute M, Raible S, Prins F E, Kern D P, Ulmer H, Weimar U and Gopel W 1999 Detection of volatile organic compounds (VOCs) with polymer-coated cantilevers *Sensors Actuators B* **58** 505–11
- [22] Yongjing L, Haitao Y, Shi G, Xiaohua G, Min L, Guomin Z, Zhenxing C and Xinxin L 2009 Hyper-branched sensing polymers self-assembled on resonant micro-cantilever sensors for ultra-low concentration DMMP vapor detection *TRANSDUCERS'09: Proc. Int. Solid-State Sensors, Actuators and Microsystems Conf.* pp 987–90
- [23] Penza M, Aversa P, Cassano G, Suriano D, Wlodarski W, Benetti M, Cannata D, Di Pietrantonio F and Verona E 2008 Thin-film bulk-acoustic-resonator gas sensor functionalized with a nanocomposite Langmuir-Blodgett layer of carbon nanotubes *IEEE Trans. Electron Devices* **55** 1237–43
- [24] Nakamoto T, Nakamura K and Moriizumi T 2000 Classification and evaluation of sensing films for QCM odor sensors by steady-state sensor response measurement *Sensors Actuators B* **69** 295–301
- [25] Sun P, Jiang Y D, Xie G Z, Du X S and Hu J 2009 A room temperature supramolecular-based quartz crystal microbalance (QCM) methane gas sensor *Sensors Actuators B* **141** 104–8
- [26] Wen W, He S T, Li S Z, Liu M H and Yong P 2007 Enhanced sensitivity of SAW gas sensor coated molecularly imprinted polymer incorporating high frequency stability oscillator *Sensors Actuators B* **125** 422–7
- [27] Hwang Y, Gao F, Hong A J and Candler R N 2012 Porous silicon resonators for improved vapor detection *J. Microelectromech. Syst.* **21** 235–42